Materials Research Proceedings 41 (2024) 192-200 https://doi.org/10.21741/9781644903131-21

Preliminary assessment of material extrusion (MEX) for medical applications: The effect of hatch angle

SALA Francesca[1,a] *, NANI Lorenzo[2,b], QUARTO Mariangela[1,c] and D'URSO Gianluca[1,d]

[1]University of Bergamo - Department of Management, Information and Production Engineering, via Pasubio 7/b, Dalmine (BG), 24044, Italy

[1]University of Bergamo - Department of Engineering and Applied Sciences, via Pasubio 7/b, Dalmine (BG), 24044, Italy

[a]francesca.sala@unibg.it, [b]lorenzo.nani@unibg.it, [c]mariangela.quarto@unibg.it, [d]gianluca.d-urso@unibg.it

Keywords: Material Extrusion, MEX, Laser Powder Bed Fusion, L-PBF, Healthcare

Abstract. Material extrusion (MEX) is one of the most widely used Additive Manufacturing (AM) technologies owing to its simplicity and accessible cost. The technique is based on the principle of extrusion of thermoplastic material, layer-by-layer, on a building platform through multiple head nozzles. Metal filled filaments, in combination with debinding and sintering cycles, may innovate and transform the traditional functioning of the MEX technique into a cost-effective alternative for the conventional metallic AM processes. In the present document, the optimal printing conditions characterizing LPBF technology were replicated on MEX technology, with the aim of assessing the effects of the printing parameter hatch angle over the material properties and, at the same time, providing a better understanding of the production of medical metal parts via MEX. Indeed, in this particular context, the use of Powder Bed Fusion (PBF) and Directed Energy Deposition (DED) prevails, requiring MEX-based technique extensive research for its applicability. The influence of a specific AM process parameter, the hatch angle, was assessed following a single factor Design of Experiment (DOE), varying over two levels: the optimal Laser Powder Bed Fusion (LPBF) scanning strategy (67°k) and the most common MEX deposition strategy (±45°). Specimens were manufactured, using MEX technology (Ultimaker S5) and AISI 316L filament (BASF Ultrafuse 316L) and tested. Results of the defect analysis, including closed and open porosity, and mechanical properties were collected and statistically compared to determine any difference in the two-deposition strategies. Furthermore, in the analysis, LPBF key characteristics are reported as benchmark values.

Introduction

The integration of metallic materials and additive manufacturing (AM) is revolutionizing the production of metal devices for medical applications. Currently, metal AM technologies, belonging to the class of Powder Bed Fusion (PBF) or Directed Energy Deposition (DED), benefit from widespread adoption in medical research. Despite its practicality and cost-effectiveness, Material Extrusion (MEX) is less adopted owing to the less control over material density and greater porosity, thereby adversely affecting the mechanical characteristics [1–3].

In the present research, Laser Powder Bed Fusion (LPBF) and MEX technologies were compared. Specifically, the optimal printing conditions characterizing LPBF technology were replicated on MEX technology, with the aim of evaluating the influence of the printing parameter hatch angle over the material properties and, at the same time, providing a better understanding of the fabrication of medical metal parts via MEX.

Optimizing and adjusting LPBF parameters have significant influences on the quality of the printed parts and the required densification, microstructure and mechanical properties [4–6]. Hence, the accomplishment of satisfactory outcomes in LPBF manufacturing relies on the balance of several factors, including laser power, scanning speed, layer thickness, hatch distance and angle. Among the process parameters, the hatch angle represents the angle of rotation with respect to the element growth axis at which scanning vectors belonging to successive layers are melted. For LPBF technologies, the optimal configuration corresponds to 67°. Thus, 67°k scanning strategy, where k indicates the number of layers, involves the rotation of each layer by 67°, creating a structure that minimizes the overlap of scanning vectors belonging to alternating layers.

Generally, the most common deposition strategy adopted by MEX processes is ±45° and it involves the deposition of material lines oriented at +45° on even layers and -45° on odd layers, commonly resulting in the overlapping phenomenon [7]. Specifically, it generates an envelope of porosity, creating continuous pores that follow the intersection of the layers along the growth direction [7]. Therefore, the objective of the current article consisted in the determination of the impact of adopting the optimal scanning strategy, distinctive of the LPBF technologies, over the key properties of elements produced with a different AM printing technique, MEX.

The current research focused on the evaluation of the influence of two different deposition strategies over MEX-built elements, in terms of tensile and hardness properties and distribution of defects (porosity). The results were assessed through statistical analysis.

The evaluations were performed on AISI 316L specimens. Stainless steel alloys are well known for their low cost and good mechanical properties, heat resistance and biocompatibility [8,9]. This material is primarily used in the fabrication of surgical instrumentation. Tough, it is relevant to note that its applications extend to orthopedic implants and fixators, artificial heart valves, syringe needles and numerous other medical tools too [10].

Methodology

Sample preparation. The test samples were produced by means of an Ultimaker S5 (Ultimaker B.V., Utrecht, NL, USA) MEX technology, using a filament with a diameter of 2.85mm provided by BASF (Ultrafuse 316L). The filament was made up of 80% austenitic stainless steel (AISI 316L) and 20% polymer content (polyoxymethylene (POM)), the latter forming the thermoplastic binder matrix that ensures material processing via MEX technology. A print core CC 0.6 with a hardened steel nozzle was used to extrude the filament.

The geometry of the specimen was designed according to international standards applicable to the mechanical tests to be performed, as further detailed in the subsequent sections.

Then, the sample geometries were imported to a slicing software, Ultimaker Cura, where the process parameters (Table 1) were defined following the optimized factors, with respect to density and shrinkage, identified in previous research [11]. Print speed was slightly increased to avoid the delamination effect in the first deposited layers, generated by the tensile specimen geometry.

Table 1. Selected process parameters for the MEX-built specimens.

	Layer height	Infill density	Infill pattern	Nozzle temperature	Build plate temperature	Print Speed
± 45°	0.1 mm	100%	± 45°	240°	100°	40 mm/s
67° k	0.1 mm	100%	67° k	240°	100°	40 mm/s

The specimens were produced following a Design of Experiment (DOE) with a single factor, planned to study the effect of two different deposition strategies. Specifically, the hatch angle, or the angle defined between the infill lines of one layer and the subsequent, was varied over two levels: ± 45° and 67°k, where k represents the layer number. Figure 1 illustrates in a layer-by-layer

comparison, the schematic representation of the two adopted deposition strategies for the core portion of the MEX-built specimens.

As anticipated, in LPBF processes, the 67°k scanning strategy is known for completely minimizing the overlap of the scanning vector of successive layers. With the adoption of the LPBF optimal strategy in MEX processes, the variation in the deposition strategy was performed by changing the infill pattern value during the set-up of the process parameters.

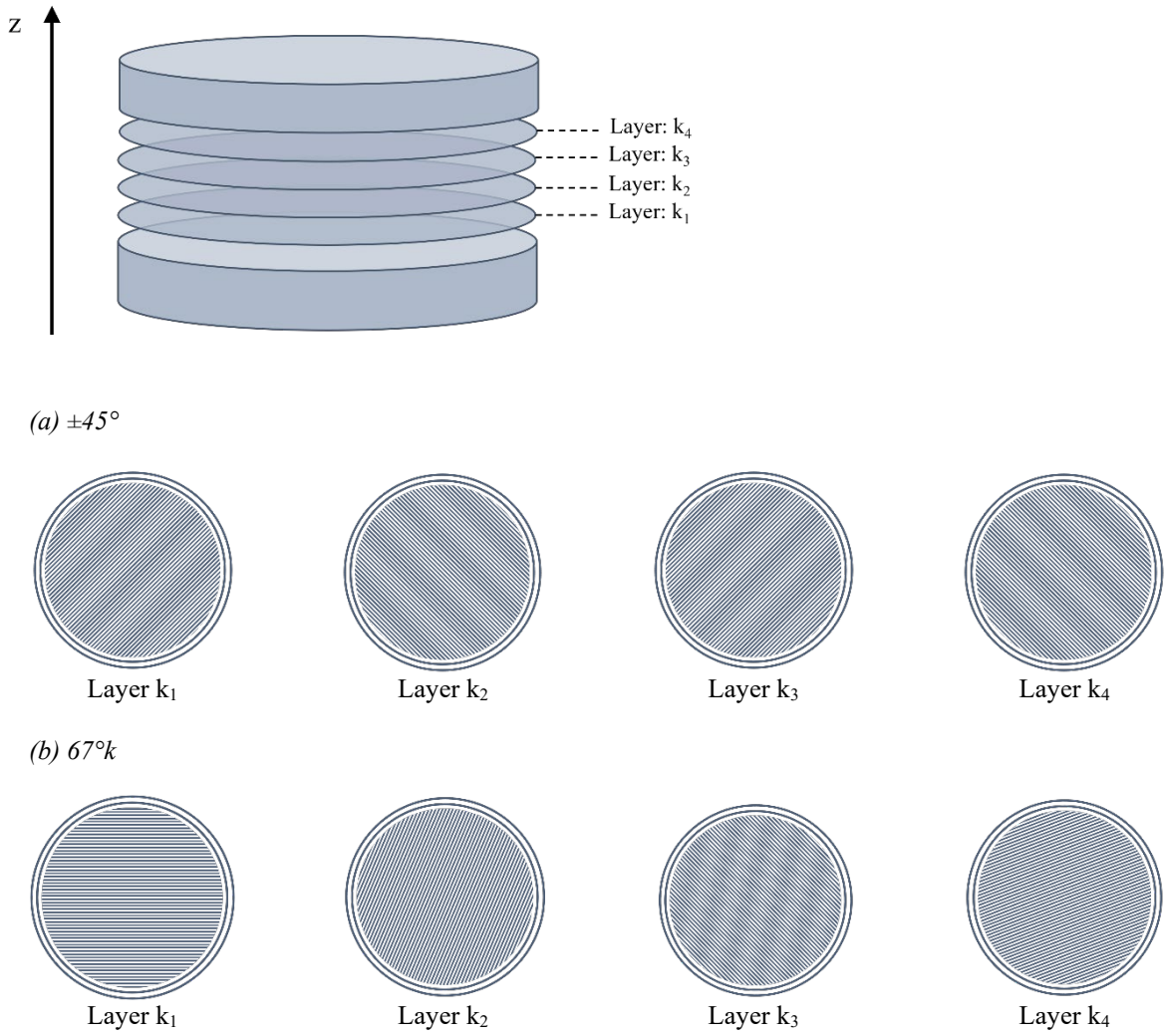

Figure 1. Layer-by-layer schematic representation of the different deposition strategies. (a) Variation of the hatch angle in four subsequent layers (+45° odd layers, -45° even layers) in ± 45° cylindrical specimen. (b) Constant variation of the hatch angle (steady rotation of 67°) in the 67°k cylindrical specimen.

Once 3D printed, the green parts underwent debinding and sintering processes to obtain, in the first instance, the brown part and, ultimately, the fully metal component. During the debinding phase, the majority of the polymeric component is removed from the green part through a catalytic and thermal process that takes place at 120°C with HNO_3 (98% concentration). During the sintering cycle, which is performed in an argon atmosphere, the brown part is subjected to three thermal ramps (Table 2). The treatments were performed by an external company.

Two sets of samples were produced and compared to benchmark values derived from literature studies and available technical datasheet on AISI 316L specimens manufactured through LPBF powders and technologies [12–16].

Table 2. Thermal ramps of the sintering cycle.

	Initial temperature	Final temperature	Ramp rate	Holding time
1st Ramp	Room temperature	600°C	5°C/min	1 h
2nd Ramp	600°C	1380°C	5°C/min	3 h
3rd Ramp	1380°C	Room temperature	Furnace cooling	

Porosity analysis. Compared to LPBF deposition processes, MEX generates structures characterized by reduced bulk density due to the presence of defects (i.e., open and closed porosity). In the present study, defect analysis was performed on cylindrical specimens with dimension 15 mm diameter and 5 mm height, in three separate stages.

In the first instance, porosities were studied by considering a cross-section orthogonal to the deposition lines (Figure 2). The surface section was polished up to 1 µm with diamond suspension. The sample sections were observed with a Keyence VHX-7100 digital-optical microscope and the amount of porosity was quantified through ImageJ software.

The metallurgical sections can only provide an indication of the porosity distribution, which is specific to identified cross-section. Given the fact that MEX processes, unlike the LPBF, tend to generate envelopes owing to the continuity of the defects between different subsequent layers rather than spherical pores, additional investigation are required. For this reason, to adequately quantify the amount of closed porosity on the whole specimen, a gas pycnometer was used. Specifically, the pycnometer estimated the average value of the volume occupied by the printed part, namely the volume of the material, and the close porosity; then, knowing the density of the material, it is possible to estimate the closed porosity as reported in Eq.1 and Eq.2.

$$\delta_{\text{bulk}} = \frac{weight}{V_{pycnometer}} \tag{1}$$

$$cp = \frac{\delta_{material} - \delta_{bulk}}{\delta material} \tag{2}$$

Where δ_{bulk} and $\delta_{material}$ are the mass density of the printed part and the material used for the printing process (8 g/cm^3) respectively, $weight$ is the mass of the printed part, $V_{pycnometer}$ is the volume of the part measured by the gas pycnometer and cp identifies the amount of closed porosity.

In a final step, an estimation of the open porosity was conducted considering the overall volume derived by the dimensions of the printed samples. In particular, the amount of open porosity (*op*) was computed as the difference between the overall volume and the volume defined by the gas pycnometer.

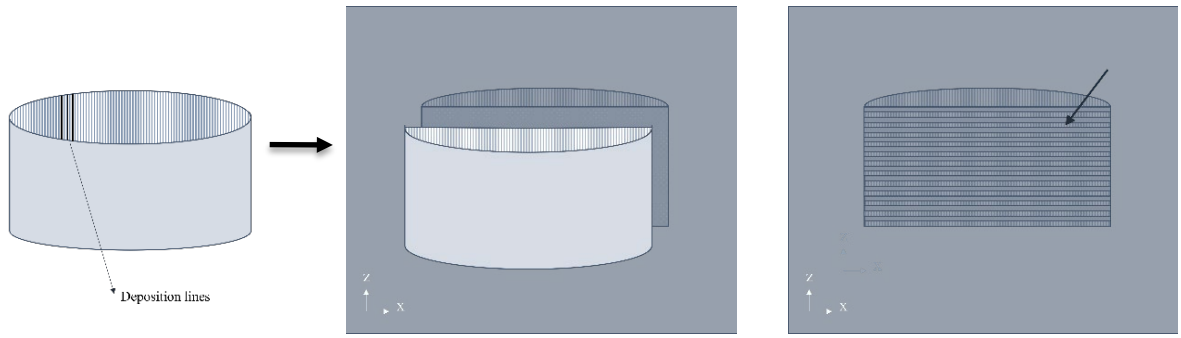

Figure 2. Schematic representation of the considered plane (cross-section parallel to the growth direction of the specimen) for the analysis of porosity.

Tensile test. According to ASTM F3122-14 [17], the procedure outlined in the test method UNI EN ISO 6892-1:2020 [18] defines the methodology for conducting a tensile test on metal materials and determining its mechanical properties, including elongation at break (A%) and ultimate tensile strengths (UTS). The procedure was performed on specimens characterized by a circular section, with a calibrated length of 30 mm and a diameter of 6 mm. Tensile tests were performed using a Galdabini testing machine with a 50kN load cell. The tests were conducted perpendicular to the growth direction of the layers, under deformation control 2.5 x 10^{-4} s^{-1} and a preload of 400N. The procedure was conducted on tensile specimens and repeated four times per deposition pattern variation.

Hardness test. ASTM F3122-14 specifies UNI EN ISO 6507-1:2018 [19] as a standard for the Vickers hardness (HV) of additive-manufactured parts. The top surface of cylindrical specimen was polished up to 1µm with diamond suspension. A 5x5 grid was drawn on the internal section, obtaining 25 uniformly spaced indentations. The procedure involved applying a 1kgf load for 15s. The protocol was repeated one time per each deposition pattern variation.

Results and discussion

Porosity analysis. The porosity analysis evaluated by means of the metallurgical sections is reported in Figure 3. The image analysis allowed to discriminate the porosity area, estimating an amount of porosity equal to 1.99% for ±45° infill pattern, and 1.47% for 67°k. For both deposition strategies, the observed porosity percentage values were reduced compared to the literature results. This result may be related to the specificity of the measurement, meaning that the value is specific to a single plane section and not directly attributable to the specimen in its entirety.

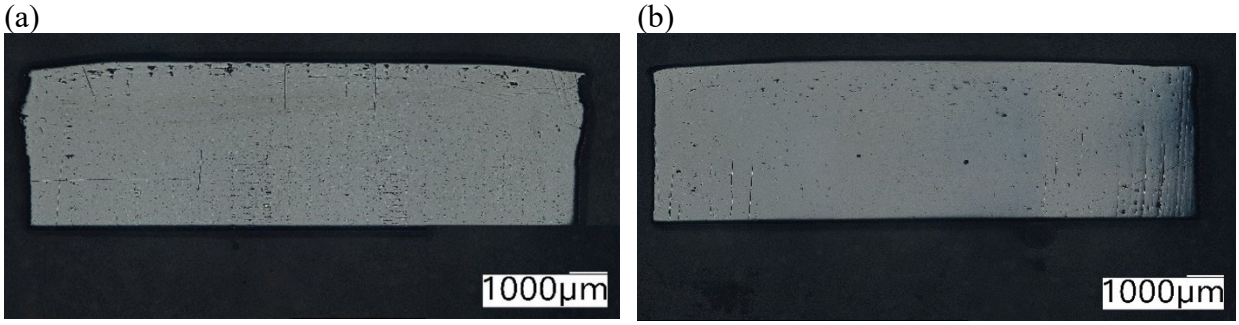

Figure 3. Metallurgical section for the two deposition strategies. (a) ±45° Infill pattern and (b) 67°k infill pattern.

The image investigation was complemented by the pycnometer analysis, which provided the aggregate value of closed porosity. The information related to the extension of the porosity along the depth dimension was captured. The pycnometer confirmed the adherence of the obtained porosity values to the conservative literature results. Furthermore, comparing the volume estimated by the gas pycnometer and the nominal part volume, the percentage of open porosity were estimated too.

The results showed that samples characterized by ± 45° infill pattern had closed porosity values of 1.29% and open porosity of 12.95%; whilst 67°k infill pattern had closed porosity values of 2.79% and open porosity of 3.70%. Although, moving from the ± 45° deposition strategy to the 67°k, the values suggested an increase in the amount of closed porosity, but a reduction considering the open porosity, prompting the ability of the 67°k to interrupt the continuity of the porosity envelope. Still, the porosity values recorded in MEX-built specimens are not comparable to the LPBF ones, capable of providing densities greater than 99%.

Tensile test. To assess the impact of the infill pattern on mechanical strength, a statistical analysis was conducted on the outcomes of tensile tests (Table 4).

The Analysis of Variance (ANOVA) showed an effect of the infill pattern on the elongation (A%) and, on the contrary, it seemed to not affect the Ultimate Tensile Strength (UTS). Notably, the elongation demonstrated a *p*-value of 0.042, which is below the predetermined confidence level of 5%. Conversely, the UTS exhibited a *p*-value of 0.951, emphasizing the absence of any substantial effect.

As reported in Figure 4, the elongation resulted to be greater for 67°k samples; this suggested that the samples 3D printed applying a 67°k pattern may undergo more deformation before reaching the point of rupture. In other words, this suggested a higher ductile behavior and greater ability to withstand deformation before necking under stress. The result may be a positive indicator for certain applications, such as when the deformability of the material is important. For example, the result may be beneficial in the medical context, where the increased ductile behavior represents improved mechanical reliability.

Table 3. Mechanical properties of tensile specimens.

Infill pattern	Repetition	A%	UTS
± 45°	1	50.5%	479 MPa
	2	47.2%	433 MPa
	3	48.4%	393 MPa
	4	40.1%	453 MPa
67°k	1	54.3%	471 MPa
	2	61.9%	439 MPa
	3	57.3%	454 MPa
	4	49.0%	400 MPa

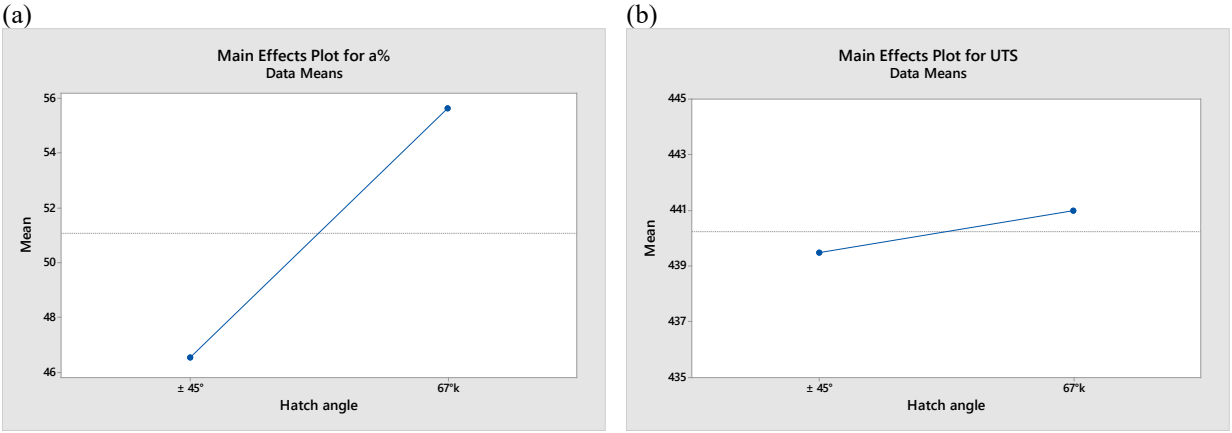

Figure 4. Main effect plot for (a) elongation at break (A%) and (b) Ultimate Tensile Strength (UTS).

Furthermore, the outcome could be correlated with the arrangement of the pores, particularly with the breaking of the envelopes caused by the continuous rotation of the pattern 67°k. This finding is supported by the images of the fracture surfaces reported in Figure 5, where it is possible to observe the distinct arrangement of the pores based on the infill pattern. It is evident that in the ± 45° infill pattern, the pores are placed along columns suggesting preferential direction for the fracture propagation, whereas for the 67°k pattern, the pores are uniformly distributed across the entire surface.

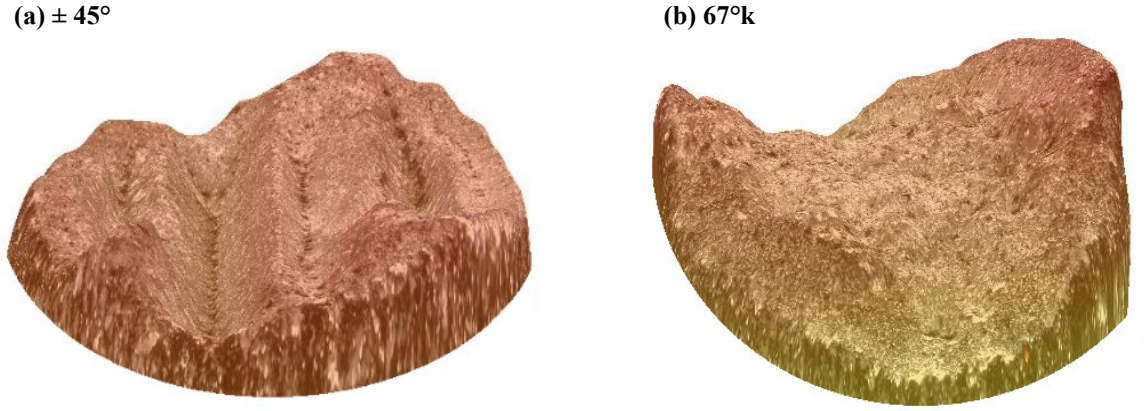

Figure 5. Reconstructions of the fracture surfaces via optical microscope. a) ± 45° Tensile specimen. b) 67° k Tensile specimen.

Table 6. Comparison of the main tensile properties measured on MEX and LPBF elements.

	MEX (± 45°)	**MEX (67° k)**	**L-PBF**
Elongation at break	46.6 ± 4.5 %	55.6 ± 5.4 %	57 %
UTS	439.5 ± 36 MPa	441.0 ± 30 MPa	Up to 700 MPa

Hardness test. In Table 7, the average values and the standard deviation of the HV_{1000} for both infill patterns were reported. It is possible to observe that there is not an appreciable difference in the values, this is probably related to the dimension of the indentation and the part structure. Specifically, the indentation is usually placed on a single strand of material, it is very difficult that the indentation involves two strand side by side, thus define a hardness that is quite similar to the monolithic one and characterized by relative low standard deviation along the entire surface.

Table 7. Comparison of the average hardness values measured on MEX and LPBF elements.

	MEX (± 45°)	**MEX (67° k)**	**LPBF**
HV_{1000} / HV	124±6 HV	131±3 HV	230 HV

Conclusion

Based on the optimized strategy defined by literature for LPBF process, the present work investigated whether, with the appropriate adaptations, the concept of an infill pattern characterized by a continuous rotation of the layers improves the structure of the parts 3D printed with metal-MEX technology. Specifically, the rotation of each layer of 67° was compared with the ±45° deposition strategy, which is the most common strategy used in MEX processes.

Cylindrical and tensile samples were manufactured modifying only the deposition strategy, via infill pattern, and the main differences in terms of porosity, tensile strength and hardness were investigated for evaluating the effectiveness of the LPBF optimal scanning strategy (67°k). The tested hypothesis consisted in the possibility of interrupting the porosity envelopes derived from the utilization of the ±45° strategy.

The relevant outcomes of the present research are summarized as follow:

- The investigated deposition strategies produced specimens with comparable total porosities; however, the porous network is significantly influenced by the deposition strategy, obtaining a periodic and semi-continuous network in the case of ±45° strategy and a fragmented network in the case of 67°k strategy.

- The differences in the porous network morphology showed negligible effects on hardness and maximum load obtained during the tensile test.
- A major effect was observed on elongation at break, where 67°k specimens withstood greater deformation before the breakage. This suggested a higher ductility derived from the optimal deposition strategy and, thus, beneficial results for applications, such as the medical ones, requiring greater predictability of fracture behavior. Additional specific investigations are required to confirm the hypothesis.

Aknowledgments
This study was carried out within the MICS (Made in Italy – Circular and Sustainable) Extended Partnership and received funding from the European Union Next-GenerationEU (PIANO NAZIONALE DI RIPRESA E RESILIENZA (PNRR) – MISSIONE 4 COMPONENTE 2, INVESTIMENTO 1.3 – D.D. 1551.11-10-2022, PE00000004). This manuscript reflects only the authors' views and opinions, neither the European Union nor the European Commission can be considered responsible for them.

References

[1] Gong, H.; Snelling, D.; Kardel, K.; Carrano, A. Comparison of Stainless Steel 316L Parts Made by FDM- and SLM-Based Additive Manufacturing Processes. *JOM* 2019, *71*, 880–885. https://doi.org/10.1007/S11837-018-3207-3/TABLES/2

[2] Kluczyński, J.; Jasik, K.; Łuszczek, J.; Sarzyński, B.; Grzelak, K.; Dražan, T.; Joska, Z.; Szachogłuchowicz, I.; Płatek, P.; Małek, M. A Comparative Investigation of Properties of Metallic Parts Additively Manufactured through MEX and PBF-LB/M Technologies. *Mater. 2023, Vol. 16, Page 5200* 2023, *16*, 5200. https://doi.org/10.3390/MA16145200

[3] Kurose, T.; Abe, Y.; Santos, M.V.A.; Kanaya, Y.; Ishigami, A.; Tanaka, S.; Ito, H. Influence of the Layer Directions on the Properties of 316l Stainless Steel Parts Fabricated through Fused Deposition of Metals. *Materials (Basel).* 2020, *13*. https://doi.org/10.3390/ma13112493

[4] Ahmed, N.; Barsoum, I.; Haidemenopoulos, G.; Al-Rub, R.K.A. Process Parameter Selection and Optimization of Laser Powder Bed Fusion for 316L Stainless Steel: A Review. *J. Manuf. Process.* 2022, *75*, 415–434. https://doi.org/10.1016/j.jmapro.2021.12.064

[5] Jia, H.; Sun, H.; Wang, H.; Wu, Y.; Wang, H. Scanning Strategy in Selective Laser Melting (SLM): A Review. *Int. J. Adv. Manuf. Technol.* 2021, *113*, 2413–2435. https://doi.org/10.1007/s00170-021-06810-3

[6] Robinson, J.H.; Robert, I.; Ashton, T.; Jones, E.; Fox, P.; Sutcliffe, C. The Effect of Hatch Angle Rotation on Parts Manufactured Using Selective Laser Melting.. https://doi.org/10.1108/RPJ-06-2017-0111

[7] Carrozza, A.; Lorenzi, S.; Carugo, F.; Fest-Santini, S.; Santini, M.; Marchese, G.; Barbieri, G.; Cognini, F.; Cabrini, M.; Pastore, T. A Comparative Analysis between Material Extrusion and Other Additive Manufacturing Techniques: Defects, Microstructure and Corrosion Behavior in Nickel Alloy 625. *Mater. Des.* 2023, *225*, 111545. https://doi.org/10.1016/J.MATDES.2022.111545

[8] Singh, R. Welding Corrosion Resistant Alloys – Stainless Steel. *Appl. Weld. Eng.* 2012, 191–214. https://doi.org/10.1016/B978-0-12-391916-8.00018-2

[9] Yang, K.; Ren, Y. Nickel-Free Austenitic Stainless Steels for Medical Applications. *Sci. Technol. Adv. Mater.* 2010, *11*, 014105. https://doi.org/10.1088/1468-6996/11/1/014105

[10] Chua, K.; Khan, I.; Malhotra, R.; Zhu, D. Additive Manufacturing and 3D Printing of Metallic Biomaterials. *Eng. Regen.* 2021, *2*, 288–299. https://doi.org/10.1016/J.ENGREG.2021.11.002

[11] Quarto, M.; Carminati, M.; D'Urso, G. Density and Shrinkage Evaluation of AISI 316L Parts Printed via FDM Process. *Mater. Manuf. Process.* 2021, *36*, 1535–1543. https://doi.org/10.1080/10426914.2021.1905830

[12] D'Andrea, D. Additive Manufacturing of AISI 316L Stainless Steel: A Review. *Met. 2023, Vol. 13, Page 1370* 2023, *13*, 1370. https://doi.org/10.3390/MET13081370

[13] Suryawanshi, J.; Prashanth, K.G.; Ramamurty, U. Mechanical Behavior of Selective Laser Melted 316L Stainless Steel. *Mater. Sci. Eng. A* 2017, *696*, 113–121. https://doi.org/10.1016/J.MSEA.2017.04.058

[14] Gatões, D.; Alves, R.; Alves, B.; Vieira, M.T. Selective Laser Melting and Mechanical Properties of Stainless Steels. *Materials (Basel).* 2022, *15*. https://doi.org/10.3390/ma15217575

[15] Xu, M.; Guo, H.; Wang, Y.; Hou, Y.; Dong, Z.; Zhang, L. Mechanical Properties and Microstructural Characteristics of 316L Stainless Steel Fabricated by Laser Powder Bed Fusion and Binder Jetting. *J. Mater. Res. Technol.* 2023, *24*, 4427–4439. https://doi.org/10.1016/J.JMRT.2023.04.069

[16] Huang, G.; Wei, K.; Deng, J.; Liu, M.; Zeng, X. High-Power Laser Powder Bed Fusion of 316L Stainless Steel: Defects, Microstructure, and Mechanical Properties. *J. Manuf. Process.* 2022, *83*, 235–245. https://doi.org/10.1016/J.JMAPRO.2022.08.066

[17] ASTM International. ASTM F3122-14 - Standard Guide for Evaluating Mechanical Properties of Metal Materials Made via Additive Manufacturing Processes 2014.

[18] International Organization for Standardization. UNI EN ISO 6892-1:2020 - Metallic Materials - Tensile Testing - Part 1: Method of Test at Room Temperature. 2020.

[19] International Organization for Standardization. UNI EN ISO 6507-1:2018 - Metallic Materials - Vickers Hardness Test - Part 1: Test Method. 2018